ACS MEASUREMENT SCIENCE Au
AN OPEN ACCESS JOURNAL OF THE AMERICAN CHEMICAL SOCIETY

pubs.acs.org/measureau

Article

Unreacted Labeled PCR Primers Inhibit the Signal in a Nucleic Acid Lateral Flow Assay as Elucidated by a Transport Reaction Model

Priyanka Agarwal and Bhushan J. Toley*

Cite This: *ACS Meas. Sci. Au* 2022, 2, 317−324

Read Online

ACCESS | Metrics & More | Article Recommendations | Supporting Information

ABSTRACT: Factors that affect the performance of the nucleic acid lateral flow assay (NALFA) have not been well studied. In this work, we identify two important phenomena that negatively affect signal intensities during the detection of PCR products using NALFA: (i) the presence of unreacted PCR primers, and (ii) the presence of excess PCR amplicons. This is the first report that highlights the negative effect of unreacted PCR primers on NALFA. The negative effect of excess amplicons, while not explicitly reported for NALFAs, emanates from an identical phenomenon in lateral flow immunoassays known as the "hook effect". We show that the above effects may be alleviated by increasing the concentration of capture antibodies at the test line and the concentration of reporter moieties (gold nanoparticles). To demonstrate these, we utilized a PCR assay in which both primers were end-labeled, to generate dually end-labeled (bi-labeled) PCR amplicons of 230 bp length. To provide mechanistic understanding of these phenomena, we present the first transport-reaction model of NALFA, the results of which qualitatively matched all observed phenomena. Based on these results, we provide recommendations for the optimal design of PCR for NALFA detection.

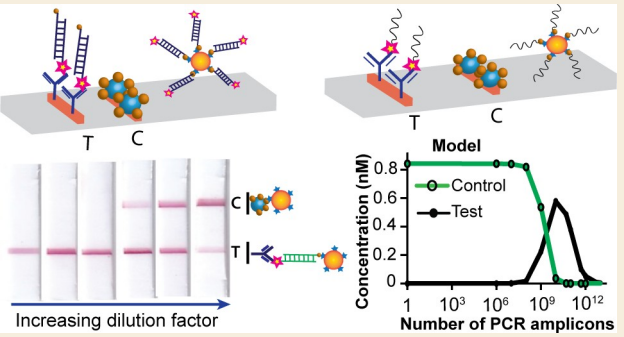

KEYWORDS: *Paper-based microfluidics, point-of-care diagnostics, hook effect, NALFA, transport phenomena, global health, tuberculosis, primer dimers*

INTRODUCTION

Point-of-care (POC) testing is essential for providing affordable healthcare worldwide as it allows rapid testing in limited-resource settings. With the global disease burden increasing, it is now crucial to develop POC compatible devices to diagnose genetic diseases and infectious and warfare agents. Lateral flow immunoassays (LFIAs) have gained attention in the field of medical diagnosis due to their convenient use, low cost, and rapid turnaround time.[1,2] Nucleic acid amplification methods are often coupled with lateral flow assays for the detection of amplification products, named as nucleic acid lateral flow assays (NALFAs).

In recent decades, the necessity for rapid and sensitive nucleic acid amplification tests (NAATs) has increased to combat pandemics like COVID-19 and to diagnose infectious diseases such as tuberculosis, malaria, etc.[3−7] Traditionally, amplified nucleic acids generated in NAATs have been detected using techniques like agarose gel electrophoresis, Southern blots, or fluorescence readouts in real-time PCR machines. All these techniques require complicated and expensive instruments and are time-consuming and labor-intensive as they involve multiple user steps and therefore are not suitable for point-of-care detection. On the other hand, NALFAs enable sensitive and specific detection of nucleic acids by simple wicking through membranes, generating a signal visible to the naked eye. So, NALFA is a powerful method that can be employed to detect amplified products of NAATs in low-middle-income countries. There are several formats of NALFA to detect DNA or RNA targets; however, the most widely used strategy is the one which involves the detection of end-labeled amplicons. Ready-to-use nucleic acid lateral flow strips have been commercialized by several manufacturers.[8−10] Bi-labeled amplicons are typically generated by using end-labeled primers or probes during the amplification process. NALFA has been coupled with several amplification methods such as polymerase chain reaction (PCR),[4,5] loop-mediated isothermal amplification (LAMP),[11,12] recombinase polymerase amplification (RPA),[13,14] and CRISPR.[15]

In practice, it has been seen that amplified nucleic acid products from PCR, LAMP, RPA ,or other isothermal amplification methods need to be diluted for a strong signal on NALFA. This dilution factor needs to be determined

Received: January 30, 2022
Revised: March 11, 2022
Accepted: March 14, 2022
Published: March 28, 2022

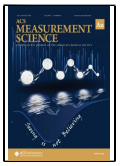

https://doi.org/10.1021/acsmeasuresciau.2c00005
ACS Meas. Sci. Au 2022, 2, 317−324

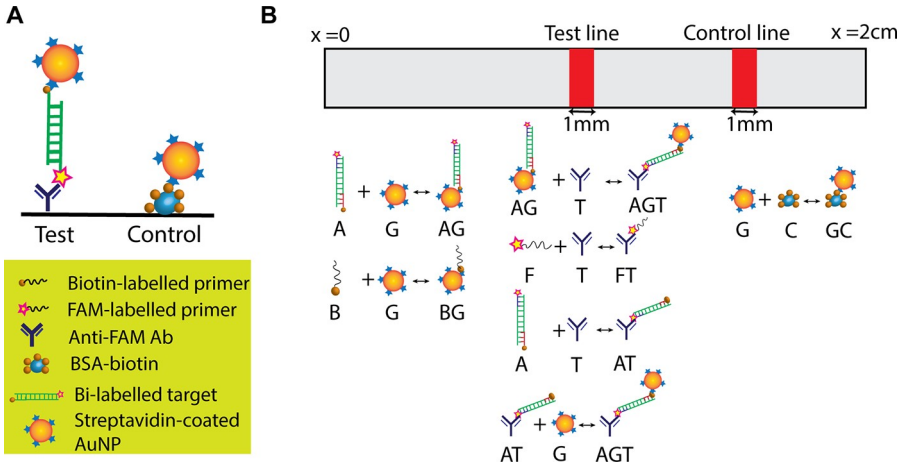

Figure 1. Design and mathematical modeling of NALFA. (A) Schematic of the nucleic acid lateral flow assay mechanism. (B) Modeling domain of nucleic acid lateral flow assay and schematics of binding reactions occurring in the domain.

experimentally by the method of trial and error. Dilution factors in the range of 10×−500× are commonly reported.[12,16−20] To date, an explanation for the need to dilute and the method to determine the optimum dilution has not been provided. Some studies also report that the NALFA signal is affected by the primer concentration used during PCR,[14,19] but the role of primer concentration is not explicitly reported in the literature. For lateral flow immunoassays, it is very well reported that the test line signal reduces with increasing analyte concentration, when the analyte concentration increases beyond a threshold concentration, popularly known as the hook effect. It could lead to reporting of false concentrations, i.e., low concentration as high, and vice versa. Several studies and mathematical models describe the hook effect, and ways to mitigate it are being explored.[13,15,21−25] However, the hook effect is not well studied for NALFAs.

In the current study, we present a first transport-reaction model of NALFA to address the above-stated knowledge gaps and to develop a better fundamental understanding of NALFAs.[26] The specific format of NALFA considered here is the one in which amplicons are generated by PCR using end-labeled primers, generating dually end-labeled (bi-labeled) amplicons. One end label is used for capture on the LFA strip, and the other end label is used to couple to a color-displaying moiety. This format is chosen because it is one of the most commonly used formats for NALFA. Using this model, we show that there are two mechanisms that adversely affect test and control line signal intensities in NALFAs: (i) the presence of labeled unreacted primers in the amplified product, and (ii) the presence of excess bilabeled DNA target (hook effect). This explains the need to dilute PCR products before NALFA; dilution alleviates both of these factors. We also show that concentrations of the reporter molecules (streptavidin-coated gold nanoparticles in this case) and test line capture antibodies play important roles in designing an optimum NALFA. This work overcomes several knowledge gaps in the design of NALFAs and will enable informed NALFA design.

EXPERIMENTAL SECTION

Materials

Albumin-biotin-labeled bovine (referred to as BSA-biotin henceforth) (A8549) and bovine serum albumin (BSA, A2153) were procured from Sigma-Aldrich. Goat polyclonal antifluorescein isothiocyanate (FITC) antibodies (ab 19224) and streptavidin-gold conjugate (40 nm, 10OD) (ab186864) were purchased from Abcam, Inc., Cambridge, MA, USA. *Mycobacterium tuberculosis* (Mtb) gDNA was obtained from BEI Resources (Manassas, VA, USA). Biotin and FAM labeled primers were purchased from Macrogen Inc., Seoul, South Korea. Takara Taq DNA Polymerase (R001A), along with buffer and deoxynucleotide triphosphates (dNTPs), was acquired from Juniper Life Sciences (Bangalore, India). dsDNA used in this study was quantified using a Nanodrop 2000 instrument (ThermoFisher Scientific). The PCR gel cleanup kit was acquired from Barcode Biosciences (Bangalore, India).

Fabrication

All materials were cut using a 50 W CO_2 laser in a VLS 3.60 laser engraver (Universal Laser Systems, Scottsdale, AZ). All designs were created in AutoCAD (Autodesk, San Rafal, CA).

Polymerase Chain Reaction Assay

A PCR assay to was designed to amplify a 230 bp region of the *rpob* gene of *Mtb*. To enable lateral flow detection of the PCR-amplified product, the 5′ ends of the forward and reverse primers were conjugated with a biotin and a FAM molecule, respectively, producing bi-labeled amplicons (Supporting Information S1). Primer sequences used in this study were forward: 5′-Biotin-ATCACACCGCAG-ACGTTGATC-3′ and reverse: 5′-FAM-GTTTCGATCGGGCACA-TCC-3′. The 20 μL PCR reaction contained 1× PCR buffer (10 mM Tris-HCl (pH8.3), 50 mM KCl, 1.5 mM $MgCl_2$), dNTP mixture (2.5 mM each), 2 units of Takara Taq DNA polymerase (rTaq r001A), 0.5 μM each of forward and reverse primers (unless otherwise stated), 1 μL of DNA template, and sterile water to occupy the remaining volume. The PCR reaction was set up with an initial denaturation at 95 °C for 5 min followed by 35 cycles of 95 °C for 30 s, 56 °C for 30 s, and 72 °C for 25 s, followed by a final extension at 72 °C for 7 min. The amplified product was detected using 1.5% agarose gel stained with ethidium bromide using gel electrophoresis.

Nucleic Acid Lateral Flow Assay

The detection mechanism of the NALFA strategy used here is shown in Figure 1A. Anti-FITC antibody was used at the test line while BSA-biotin at the control line. For this study, conjugate pads were not used; instead, streptavidin-gold nanoparticles (Sv-AuNPs) were premixed with the sample and introduced directly into the lateral flow strip. Sv-AuNPs were diluted in conjugate buffer (2 mM borate buffer, 10% sucrose, pH 7), while target amplicons were diluted in running buffer (0.01 M PBS (phosphate buffered saline), 1% BSA, 0.05% Tween-20, pH 7.4). NALFA was fabricated as described in Supporting Information S2. NALFA was conducted with two types of samples: (i) directly on PCR products and (ii) on purified PCR amplicons obtained using the gel cleanup kit. Purified amplicons were free of unreacted primers and so were useful in validating certain

https://doi.org/10.1021/acsmeasuresciau.2c00005
ACS Meas. Sci. Au 2022, 2, 317−324

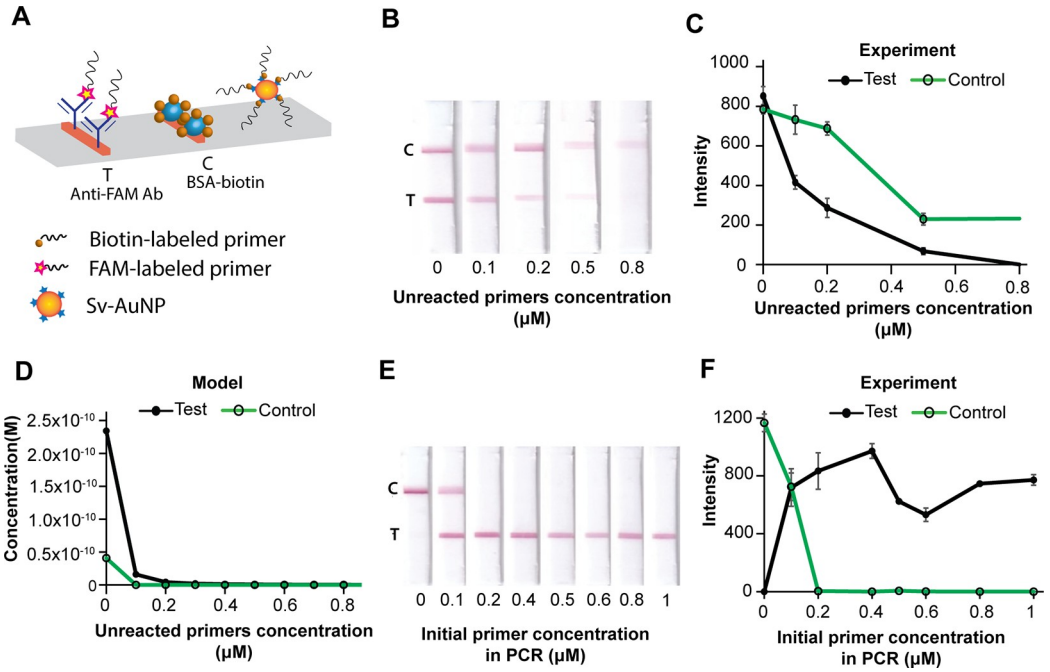

Figure 2. Signal inhibition due to unreacted primers. (A) Schematic showing the effect of unreacted primers on NALFA chemistry. (B) Images of NALFA strips conducted for purified PCR amplicons spiked with varying concentrations of unreacted primers. (C) Plots of test and control line intensities vs concentration of unreacted primers obtained experimentally. (D) Plots of test and control line concentrations vs concentration of unreacted primers obtained using the model. (E) NALFA images at various initial primer concentrations in polymerase chain reaction. (F) Plots of test and control line intensities vs initial concentration of primers in PCR. All error bars represent standard deviations (N = 3).

aspects of the mathematical model. The concentration (ng/μL) of purified amplicons was measured using the Nanodrop 2000 instrument and converted to copy number using the molecular weight of the amplicons (Supporting Information S3). The OD 260/280 purity ratio was maintained between 1.8 and 2 to ensure purity of amplicons. The BSA-biotin concentration was 0.5 mg/mL in all the experiments, unless stated otherwise. The anti-FITC antibody concentration was 0.25 mg/mL for experiments showing inhibition of test and control line signal using purified amplicons, 0.5 mg/mL for experiments conducted with PCR product using different primer concentrations and experiments with varying BSA-biotin concentration, and 1 mg/mL for experiments involving the hook effect and effect of reporter moiety concentration.

Image Analysis

A flatbed scanner was used to quantify the signal generated in NALFA. Images were acquired 12 min after sample introduction. Each image was split into red, green, and blue channels using ImageJ. The green channel provided the highest contrast against the background (Figure S3); hence, green channel intensities were recorded. The intensity vs distance data from ImageJ was imported to MATLAB, and a custom MATLAB script was used to identify and measure the integrated intensities of test and control lines (Supporting Information S4).

Modeling Section

Transport-reaction phenomena within NALFA were modeled. There are two important length scales at which transport phenomena occur in NALFA: (i) the macroscopic transport of bulk liquid from the source well to the reaction zones (test and control lines), and (ii) the microscopic transport of species within individual pores from the bulk to the surface for subsequent reaction. For microscopic transport, the diffusion of molecules to the surface (transverse to the direction of convective flow) is significantly faster than the surface reaction. Reactions in the test and control zones may therefore be modeled as bulk reactions rather than surface reactions. This enables reducing the model to a 1D model that only considers macroscopic transport phenomena. At the macroscopic length scale, both convection and dispersion (modified diffusion as a result of heterogeneous pores in the porous medium) contribute to transport. However, convection dominates at these length scales (Peclet number $\sim 10^3$).[27] While dispersion is not ignored in this model, it is replaced by molecular diffusion, which is an approximation of the rate of dispersion.

The nitrocellulose membrane consisting of the test and control line was considered as the modeling domain. The length of the domain was 2 cm and the widths of the test and control lines were 1 mm (Figure 1B). The capture antibody (anti-FITC) at the test line (T) and BSA-biotin at the control line (C) were assumed to be immobilized homogeneously at their respective locations. Sample containing bi-labeled amplicons (A), biotin-labeled primers (B), and FAM-labeled primers (F) was diluted in running buffer and premixed with Sv-AuNPs (reporter molecules, G). This mixture was assumed to flow through the domain at a constant velocity,[27] v. The assumption of constant velocity is valid because after the nitrocellulose strip wets fully and the fluid front enters the wicking pad, the flow rate remains nearly constant for a long period of time.[27] Note that the model assumes that Sv-AuNPs, anti-FITC antibody, and BSA-biotin have only one binding site.

The binding reactions which occur in NALFA are represented in Figure 1B. All chemical reactions were assumed to be reversible. Bi-labeled amplicons (A) and biotin-labeled primer present in the sample binds with the reporter label (G) to form an amplicon-reporter complex (AG; A + G $\rightleftarrows$ AG) and biotin primer-reporter complex (BG; B + G $\rightleftarrows$ BG), respectively. At the test line, anti-FITC antibody (T) captures the amplicons (A), FAM-labeled primer (F), and amplicon–reporter complex (AG), forming the amplicon–antibody complex (AT; A + T $\rightleftarrows$ AT), FAM primer–antibody complex (FT; F + T $\rightleftarrows$ FT), and amplicon–reporter–antibody complex (AGT; AG + T $\rightleftarrows$ AGT), respectively. Free reporter molecules (G) interact with amplicon-antibody complex (AT) to also form an amplicon-reporter-antibody complex (AGT; AT + G $\rightleftarrows$ AGT). The signal at the test line is due to the formation of species AGT. Unbound reporter molecules (G) are captured at the control line by BSA-biotin (C) to form a complex GC; G + C $\rightleftarrows$ GC, which is responsible for the control line signal development.

https://doi.org/10.1021/acsmeasuresciau.2c00005
ACS Meas. Sci. Au 2022, 2, 317–324

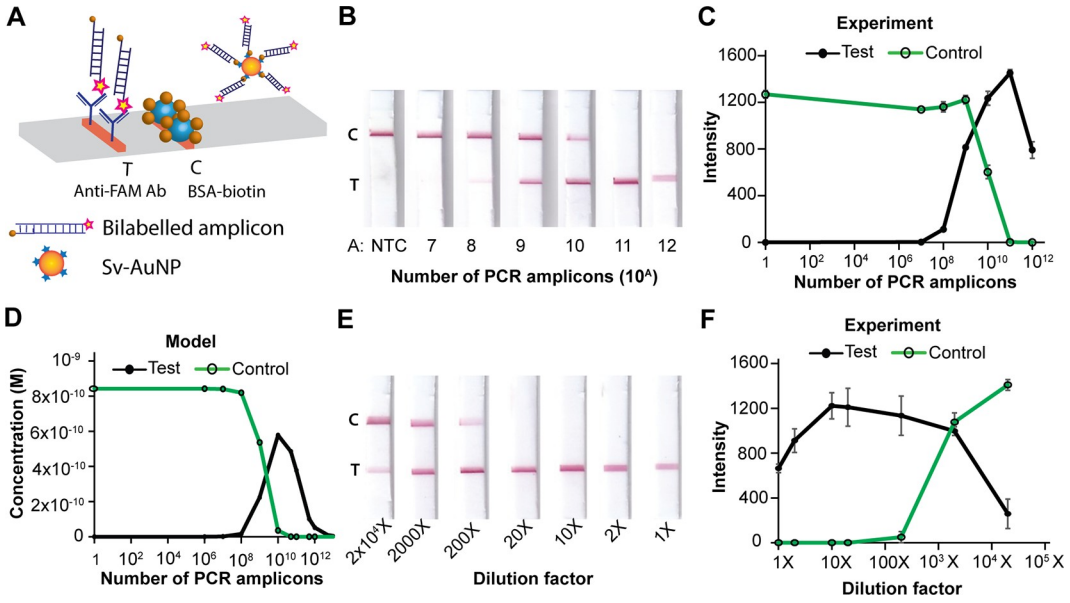

Figure 3. Hook effect in NALFA. (A) Schematic for the mechanism of loss of test and control line intensities when bi-labeled amplicons are in excess. (B) NALFA conducted with increasing number of purified PCR amplicons. (C) Plots of test and control line intensities vs number of amplicons obtained experimentally using purified amplicons. (D) Plots of test and control line concentrations vs number of amplicons obtained using the model. (E) NALFA conducted from serial dilutions of PCR products. (F) Plots of test and control line intensities vs number of amplicons obtained experimentally from serial dilutions of PCR product. All error bars represent standard deviations (N = 3).

The mathematical model involves a diffusion−convection reaction equation for all the species, which is given as follows:

$$\frac{\partial C_i}{\partial t} = D_i \frac{\partial C_i^2}{\partial x^2} - \nu\left(\frac{\partial C_i}{\partial x}\right) + F_i; \quad i = \text{A, B, G, F, AG, BG} \tag{1}$$

$$\frac{\partial C_i}{\partial t} = F_i; \quad i = \text{AT, FT, AGT, GC} \tag{2}$$

where C_i is the concentration of species i, D_i is the effective diffusivity for the i^{th} species in water, ν is the fluid flow velocity, and F_i is the rate of formation for the i^{th} species. The effective diffusion coefficient is lower than the diffusion coefficient of reagents in the free liquid due to the porous nature of the nitrocellulose membranes. Because surface-bound species cannot undergo convection or diffusion, they are represented by eq 2 while all other free species are represented by eq 1. The complete list of equations, the initial and boundary conditions, and the values of parameters used in the model (diffusivities, reaction rate constants, and fluid flow velocity) is given in Supporting Information S5. Using finite central differences, the set of coupled partial differential equations was discretized to generate a set of ordinary differential equations. These were then solved in MATLAB using the inbuilt ode15s solver for stiff ODEs to obtain the concentration of all species over space and time. To produce a movie of a simulated NALFA, the total concentration of signal-forming species at the test and control lines was scaled to between 0 and 255 and the scaled numbers were used to generate the red color over a white background.

RESULTS AND DISCUSSION

Unreacted Primers Inhibit Test and Control Line Signals

The designed 35 cycle PCR assay could detect as few as 10 copies/reaction on 1.5% agarose gel and generate a 230 bp product (Figure S5). It was first observed that when PCR was cut short, i.e., stopped after 20 cycles, and NALFA was conducted using these products, it led to a near loss of signal at the test and control lines (Supporting Information S6). While the loss of signal at the test line may have been due to a low product concentration from the incomplete PCR, there was no obvious explanation for the loss of signal at the control line. We hypothesized that this loss in signal was because of the presence of unreacted PCR primers by the following mechanism. When a significant concentration of unreacted PCR primers is present in the sample (Figure 2A), FAM-labeled primers would block the anti-FITC antibody reaction sites on the test line, reducing the available number of binding sites for the reporter-bound amplicons to bind. Similarly, biotin-labeled primers would block streptavidin sites on Sv-AuNPs, reducing the available number of particles for signal generation at both test and control lines (Figure 2A).

To test the hypothesis that unreacted PCR primers inhibit signals on test and control lines, gel-purified bi-labeled PCR amplicons were spiked with different concentrations of primers (in the range of 0−0.8 μM) and used for NALFA. The number of amplicons (10^{10} copies) was kept unaltered. Ten μL of 1 OD gold conjugate solution was premixed with the amplicons. Both the test and control signal intensities reduced with increasing unreacted primer concentrations (Figure 2B,C). A dark signal was generated in the absence of unreacted primers. However, the test line was lost completely in the presence of 0.8 μM unreacted primers (Figure 2B,C). The control line intensity also dropped ∼3.5× with increasing unreacted primer concentration from 0 to 0.8 μM (Figure 2B,C). Modeling results showed a similar trend of reducing test and control line intensities when the concentration of unreacted primers was increased from 0−0.8 μM (Figure 2D). A movie of a simulated NALFA using the mathematical model is provided in the Supporting Information (Movie S1).

The effect of unreacted primers was then demonstrated by performing NALFA directly on PCR products. PCR was performed with different initial primer concentrations varying from 0 to 1 μM, keeping the initial target concentration constant, i.e., 1000 copies of *Mtb* genomic DNA. One μL of PCR product was then diluted to 30 μL in running buffer and was premixed with 10 μL of 1.5 OD gold conjugate solution.

https://doi.org/10.1021/acsmeasuresciau.2c00005
ACS Meas. Sci. Au 2022, 2, 317−324

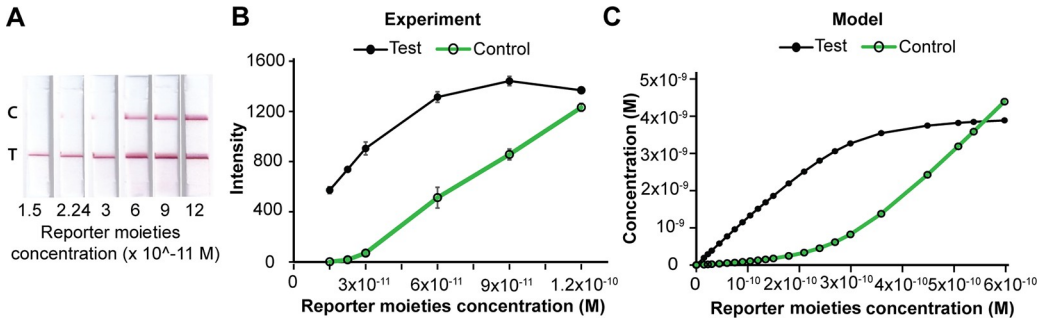

Figure 4. Effect of the concentration of reporter moieties (Sv-AuNPs). (A) Images of NALFA conducted with varying amounts of Sv-AuNPs. (B) Plots of test and control line intensities vs gold nanoparticle concentration obtained experimentally. (C) Plots of test and control line concentrations vs gold nanoparticle concentration obtained from the model. All error bars represent standard deviations (N = 3).

This premixed sample was then used for NALFA. The control line intensity decreased with increasing primer concentration (Figure 2E). The test line intensity increased as the primer concentration was increased from 0−0.4 μM (Figure 2E,F). This is because of the obvious reason for increasing PCR product formed with increasing primer concentration. On further increasing the primer concentration from 0.4 to 0.6 μM, the test line intensity started dropping (Figure 2E,F). This is because although the number of bi-labeled amplicons increased, the number of free primers also increased, which adversely affected test line signal. Interestingly, on further increasing primer concentration (0−1 μM), the test line intensity increased again. This was most likely because of the formation of primer-dimers at very high primer concentration, which also happen to be bi-labeled products of amplification, and lead to false positives on NALFA. This was confirmed in a separate experiment by performing PCR using varying primer concentrations in the absence of a template. Ideally, the test line should not appear on NALFA because there was no target to be amplified. Contrarily, a test line appeared for all primer concentrations in the range of 0.4−1 μM, as shown in Figure S7A. To rule out the possibility of amplicon contamination, 2 μL of PCR product generated from a no-template reaction was analyzed using agarose gel (Figure S7B), where no target-specific band appeared. Overall, these results show that there is an optimal range of PCR primer concentrations for best performance of NALFA. Below a certain primer concentration, the product concentration may be too low to produce a dark signal. Above a threshold primer concentration, the signal drops because of the presence of unreacted primers. At very high primer concentrations, NALFA may begin to show nonspecific signals (from primer dimers).

Hook Effect

When bi-labeled amplicons are present in excess, it reduces the probability of forming the full detectable stack at both the test and control lines (Figure 3A). Some amplicons completely cover the AuNPs, leaving no valency for AuNPs to bind to the control line, reducing control line signals; other amplicons occupy test line antibody sites without any gold nanoparticles bound to them, reducing test line signals.

To demonstrate the effect of excess amplicons, different concentrations of bi-labeled PCR amplicons (ranging from 10^7 to 10^{12} copies and a blank) were analyzed using NALFA (Figure 3B,C). As the number of amplicons increased until 10^{11} copies, the test line intensity increased; however, at 10^{12} copies, the test line intensity reduced (Figure 3B,C). This is identical to the hook effect, an effect well-known to occur in lateral flow immunoassays. The control line intensity remained largely unaltered at low amplicon concentrations, but it rapidly declined at very high amplicon concentrations (Figure 3B,C). The results of the mathematical model matched the experimental observation qualitatively (Figure 3D). In this case, there were no unreacted primers present in the sample.

The hook effect was next demonstrated by conducting NALFA directly on PCR products obtained from amplifying 1000 copies of target. Ten μL of 1.5 OD gold conjugate solution was used for detection. In this case, multiple serial dilutions (1×, 2×, 10×, 20×, 2000×, and 20 000×) of the PCR product were used for NALFA. In the case of undiluted PCR product (1×), only the test line appeared due to complete the utilization of available reporter molecules by the amplicons (Figure 3E,F). As the dilution factor increased until 10×, the test line signal intensity increased because of alleviation of the hook effect. On further dilution beyond 10×, the test line intensity reduced because of less availability of bi-labeled target (Figure 3E,F). The control line appeared only for dilutions of 200× and above, at which point Sv-AuNPs were not completely consumed by bi-labeled amplicons and were hence available for binding to the control line (Figure 3E,F). These results corroborate the need to dilute PCR amplicons before NALFA.

Effect of Concentration of Reporter Moieties

The accumulation of reporter moieties at test and control lines is responsible for signal generation in lateral flow assays; the signal increases with increasing concentration of reporter moieties accumulated. In this study, 40 nm Sv-AuNPs were used as reporter moieties. The effect of concentration of gold nanoparticles was studied by running NALFA assays with varying gold nanoparticle concentrations and all other parameters unaltered. NALFAs were run with 10^{10} copies of purified target dsDNA without any free primers. A 10 μL solution of gold nanoparticles was mixed with the amplicon solution before NALFA; the optical density (OD) of the gold conjugate was varied from 0.5 to 4, which corresponded to 1.49×10^{-11}−1.2×10^{-10} M. As the concentration of gold nanoparticles was increased, the test line signal increased and then plateaued at higher concentrations; the control line signal was initially not visible, and subsequently increased monotonously (Figure 4A,B). Results from the model matched these trends qualitatively (Figure 4C). At high gold nanoparticle concentrations, the test line signal saturates because all sites for binding on the line are occupied. Overall, increasing the concentration of gold nanoparticles has a positive impact on NALFA performance. The trade-off, however, comes from the

https://doi.org/10.1021/acsmeasuresciau.2c00005
ACS Meas. Sci. Au 2022, 2, 317−324

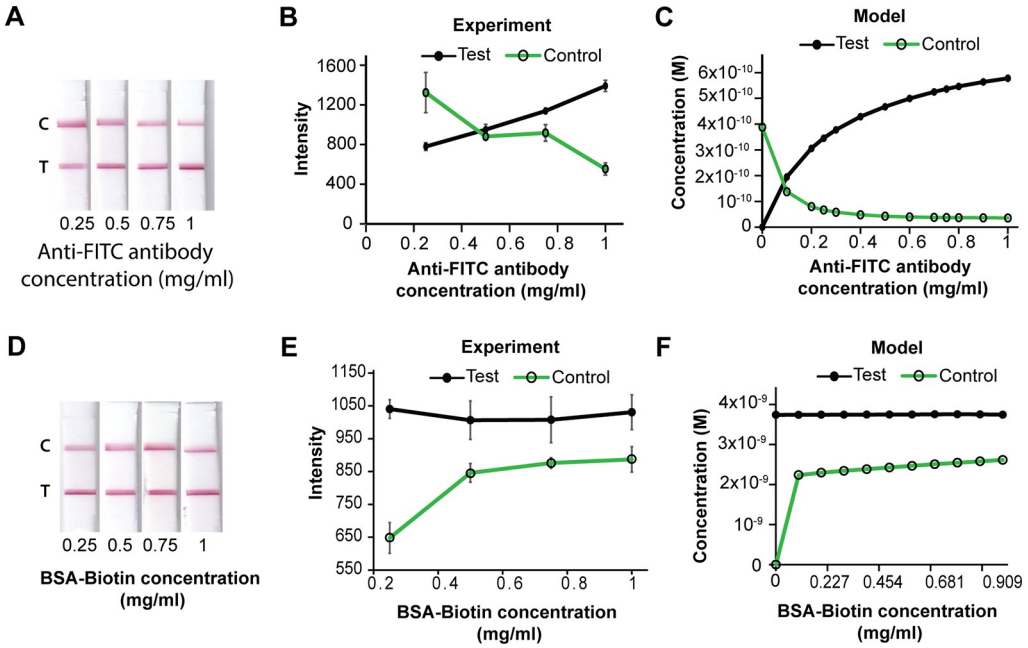

Figure 5. Effects of concentrations of test and control line capture molecules. (A) Images of NALFA conducted with varying concentrations of anti-FITC antibody at the test line. (B) Plots of test and control line intensities vs anti-FITC antibody concentration obtained experimentally. (C) Plots of test and control line concentrations vs anti-FITC antibody concentration obtained from the model. (D) Images of NALFA conducted with varying concentrations of BSA-biotin at the control line. (E) Plots of test and control line intensities vs BSA-biotin concentration obtained experimentally. (F) Plots of test and control line concentrations vs BSA-biotin concentration obtained from the model. All error bars represent standard deviations (N = 3).

cost of the reporter moieties. Sv-AuNPs, for example, could add to the cost of NALFA substantially; the Abcam particles used here cost ~$0.90/1 μL solution of 10 OD. Further, although not common for streptavidin-coated gold nanoparticles, in case there is any nonspecific binding of nanoparticles to test line antibodies, high gold nanoparticle concentrations may lead to target-independent signals on the test line. It is therefore important to utilize the lowest number of nanoparticles that provide the required sensitivity in NALFA.

Effect of Anti-FITC Antibody Concentration (Test Line) and BSA-Biotin Concentration (Control Line)

In order to study the effect of the concentration of anti-FITC antibody at the test line, NALFAs were run with 10^{10} copies of bi-labeled amplicons, mixed with 10 μL of 1.5 OD Sv-AuNPs. When the concentration of anti-FITC antibody at the test line was increased from 0.25 to 1 mg/mL, keeping all other parameters constant, the test line signal improved. This can be attributed to enhancement in binding kinetics at the test line (Figure 5A,B). In most lateral flow assays, the rate of binding of the detectable entity is less than the rate of convection (flow over test line). Many detectable molecules, therefore, flow past the test line without binding. Increasing the concentration of test line antibodies alleviates this issue. On the contrary, when the concentration of anti-FITC antibody at the test line was increased, the control line signal reduced because higher amounts of reporter moieties were now consumed at the test line and thus less were available to bind to the control line (Figure 5A,B). Results of the mathematical model matched these trends qualitatively (Figure 5C). Identical NALFAs were conducted to study the effect of the concentration of BSA-biotin at the control line. When the concentration of BSA-biotin was increased from 0.25 to 1 mg/mL, keeping all other parameters constant, the control line intensity increased and then plateaued (Figure 5D,E). The test line intensity remained unchanged as expected (Figure 5D,E) because modifications at the control line do not affect any phenomena at the test line, which us upstream the control line. Results from the mathematical model showed similar trends (Figure 5F). Overall, these results show that increasing the concentration of the capture molecule at the test line may be used to improve signals at the test line. Similar arguments about trade-offs associated with costs and nonspecific signals at the test line may be made; antibodies may contribute significantly to the total cost of NALFA.

Overall, we have shown that the test and control line signal intensities strongly depend on the design of the PCR assay (primer concentration and number of cycles) and the concentrations of the reporter moiety and capture molecules used at the test and control lines. The dilution of products of amplification, as reported in NALFA literature, is necessary to alleviate the hook effect as well as loss of signal because of the presence of unreacted primers. The results presented here will hold true for NALFA detection of any nucleic acid amplification method utilizing labeled primers. Because this study analyzes the factors that affect the intensity of lateral flow signals, it will significantly aid in the design of quantitative/semiquantitative NALFA strategies. The modeling strategy used in this study makes the simplifying assumption that each Sv-AuNP has only a single valency for biotin. In reality, each Sv-AuNP has multiple valencies for biotin. Further, because a calibration of signal intensities at test and control lines vs the number of gold nanoparticles accumulated to generate the signal was not performed, an exact quantitative comparison of experimental vs modeling results was not possible. However, because the purpose of the model was to obtain qualitative trends, the current model suffices for the purpose.

https://doi.org/10.1021/acsmeasuresciau.2c00005
ACS Meas. Sci. Au 2022, 2, 317−324

CONCLUSION

To date, the design of NALFAs has largely employed a black box approach; a few published protocols have been adopted by most researchers without knowledge of the factors that affect its performance. In this work, we recognize multiple factors that affect the performance of NALFAs and provide a mechanistic explanation for them by utilizing a mathematical model. An important outcome of this work is the understanding that unreacted PCR primers inhibit the signal in NALFA, which necessitates that PCR be run until the end point before utilizing NALFA as a readout method. We also highlight the hook effect that reduces the NALFA signal and prove that this effect necessitates dilution of the amplicons prior to NALFA, as is commonly reported in NALFA protocols. This result has important implications in the design of integrated devices that aim to directly couple a PCR reaction to NALFA, where dilution of amplicons may not be feasible. In such cases, we show that increasing the concentration of test line antibodies and the reporter moieties may alleviate signal inhibition. This work also brings forth the following important factors that must be considered for the optimal design of PCR for NALFA detection: (i) PCR must be designed with limiting primer concentrations to ensure that there are no unreacted primers at the end of the reaction; i.e., there must be an excess of dNTPs in the reaction; (ii) PCR should not be terminated prior to the designated number of cycles, even though a detectable concentration of product may have been generated; and (iii) to facilitate the detection of undiluted PCR products using NALFA, the primer concentrations must be chosen to be as low as possible to not run into the high analyte concentration hook effect regime but not so low to negatively impact PCR efficiency.

ASSOCIATED CONTENT

Supporting Information

The Supporting Information is available free of charge at https://pubs.acs.org/doi/10.1021/acsmeasuresciau.2c00005.

Labeling of PCR primer; fabrication of nucleic acid lateral flow assay (NALFA); conversion of DNA concentration to copy number; image analysis; mathematical model equations; nucleic acid lateral flow detection after cutting off PCR at 20 cycles; false positives on NALFA due to primer dimers (PDF)

Movie of a simulated NALFA using the mathematical model (AVI)

AUTHOR INFORMATION

Corresponding Author

Bhushan J. Toley − *Department of Chemical Engineering and Center for Biosystems Science and Engineering, Indian Institute of Science, Bengaluru, Karnataka 560012, India;* orcid.org/0000-0003-0119-2350; Phone: +91-80-2293-3114; Email: bhushan@iisc.ac.in

Author

Priyanka Agarwal − *Department of Chemical Engineering, Indian Institute of Science, Bengaluru, Karnataka 560012, India*

Complete contact information is available at: https://pubs.acs.org/10.1021/acsmeasuresciau.2c00005

Notes

The authors declare no competing financial interest.

ACKNOWLEDGMENTS

This work was supported by an extramural research grant from the Science and Engineering Research Board, India (EMR/2016/006029), an Innovative Young Biotechnologist award from the Department of Biotechnology, India (BT/010/IYBA/2016/07), a special grant from the DBT-BIRAC COVID19 consortium (BT/PR40322/COD/139/10/2020), a Grand Challenges Exploration-India award from BIRAC-India, and by the Saroj Poddar Foundation in the form of a Young Investigator award, all to B.J.T. We would like to acknowledge valuable contributions from Mr. Vishnu Kumar in PCR assay design, support from Mr. N. Sathishkumar on the MATLAB script for simulation, and valuable inputs on the mathematical model from Prof. V. Kumaran.

REFERENCES

(1) Koczula, K. M.; Gallotta, A. Lateral Flow Assays. *Essays in Biochemistry* **2016**, *60* (1), 111−120.

(2) Hsieh, H.; Dantzler, J.; Weigl, B. Analytical Tools to Improve Optimization Procedures for Lateral Flow Assays. *Diagnostics* **2017**, *7* (2), 29.

(3) Reboud, J.; Xu, G.; Garrett, A.; Adriko, M.; Yang, Z.; Tukahebwa, E. M.; Rowell, C.; Cooper, J. M. Paper-Based Microfluidics for DNA Diagnostics of Malaria in Low Resource Underserved Rural Communities. *Proc. Natl. Acad. Sci. U.S.A.* **2019**, *116* (11), 4834−4842.

(4) Amalina, Z. N.; Khalid, M. F.; Rahman, S. F.; Ahmad, M. N.; Najib, M. A.; Ismail, A.; Aziah, I. Nucleic Acid-Based Lateral Flow Biosensor for Salmonella Typhi and Salmonella Paratyphi: A Detection in Stool Samples of Suspected Carriers. *Diagnostics* **2021**, *11* (4), 700.

(5) Seidel, C.; Peters, S.; Eschbach, E.; Feßler, A. T.; Oberheitmann, B.; Schwarz, S. Development of a Nucleic Acid Lateral Flow Immunoassay (NALFIA) for Reliable, Simple and Rapid Detection of the Methicillin Resistance Genes MecA and MecC. *Vet. Microbiol.* **2017**, *200*, 101−106.

(6) Zhou, Y.; Wu, Y.; Ding, L.; Huang, X.; Xiong, Y. Point-of-Care COVID-19 Diagnostics Powered by Lateral Flow Assay. *TrAC, Trends Anal. Chem.* **2021**, 116452.

(7) Niemz, A.; Boyle, D. S. Nucleic Acid Testing for Tuberculosis at the Point-of-Care in High-Burden Countries. *Expert Review of Molecular Diagnostics* **2012**, *12* (7), 687−701.

(8) Nucleic Acid Lateral Flow Kit. *DCN Dx*. https://dcndx.com/store/product/nucleic-acid-lateral-flow-kit/ (accessed 2022- 01-27).

(9) PCRD. *Abingdon Health plc*. https://www.abingdonhealth.com/products/pcrd/ (accessed 2022-01-27).

(10) HybriDetect - Universal Lateral Flow Test Strips. *Milenia Biotec*. https://www.milenia-biotec.com/en/product/hybridetect/ (accessed 2022-01-27).

(11) Li, S.; Liu, Y.; Wang, Y.; Chen, H.; Liu, C.; Wang, Y. Lateral Flow Biosensor Combined with Loop-Mediated Isothermal Amplification for Simple, Rapid, Sensitive, and Reliable Detection of Brucella Spp. *Infection and Drug Resistance* **2019**, *12*, 2343−2353.

(12) Zhang, J.; Cao, J.; Zhu, M.; Xu, M.; Shi, F. Loop-Mediated Isothermal Amplification-Lateral-Flow Dipstick (LAMP-LFD) to Detect Mycoplasma Ovipneumoniae. *World J. Microbiol. Biotechnol.* **2019**, *35* (2), 31.

(13) Safenkova, I. v.; Ivanov, A. v.; Slutskaya, E. S.; Samokhvalov, A. v.; Zherdev, A. v.; Dzantiev, B. B. Key Significance of DNA-Target Size in Lateral Flow Assay Coupled with Recombinase Polymerase Amplification. *Anal. Chim. Acta* **2020**, *1102*, 109−118.

(14) Ivanov, A. v.; Safenkova, I. v.; Zherdev, A. v.; Dzantiev, B. B. Nucleic Acid Lateral Flow Assay with Recombinase Polymerase

Amplification: Solutions for Highly Sensitive Detection of RNA Virus. *Talanta* **2020**, *210*, 120616.
(15) Azhar, M.; Phutela, R.; Kumar, M.; Ansari, A. H.; Rauthan, R.; Gulati, S.; Sharma, N.; Sinha, D.; Sharma, S.; Singh, S.; Acharya, S.; Sarkar, S.; Paul, D.; Kathpalia, P.; Aich, M.; Sehgal, P.; Ranjan, G.; Bhoyar, R. C.; Singhal, K.; Lad, H.; Patra, P. K.; Makharia, G.; Chandak, G. R.; Pesala, B.; Chakraborty, D.; Maiti, S. Rapid and Accurate Nucleobase Detection Using FnCas9 and Its Application in COVID-19 Diagnosis. *Biosens. Bioelectron.* **2021**, *183*, 113207.
(16) Tomlinson, J. A.; Dickinson, M. J.; Boonham, N. Rapid Detection of Phytophthora Ramorum and P. Kernoviae by Two-Minute DNA Extraction Followed by Isothermal Amplification and Amplicon Detection by Generic Lateral Flow Device. *Phytopathology* **2010**, *100* (2), 143−149.
(17) Doyle, J.; Uthicke, S. Sensitive Environmental DNA Detection via Lateral Flow Assay (Dipstick)—A Case Study on Corallivorous Crown-of-Thorns Sea Star (Acanthaster Cf. Solaris) Detection. *Environmental DNA* **2021**, *3* (2), 323−342.
(18) Ang, G. Y.; Yu, C. Y.; Yean, C. Y. Ambient Temperature Detection of PCR Amplicons with a Novel Sequence-Specific Nucleic Acid Lateral Flow Biosensor. *Biosens. Bioelectron.* **2012**, *38* (1), 151−156.
(19) Jauset-Rubio, M.; Svobodová, M.; Mairal, T.; McNeil, C.; Keegan, N.; Saeed, A.; Abbas, M. N.; El-Shahawi, M. S.; Bashammakh, A. S.; Alyoubi, A. O.; O'Sullivan, C. K. Ultrasensitive, Rapid and Inexpensive Detection of DNA Using Paper Based Lateral Flow Assay. *Sci. Rep.* **2016**, *6*, 37732.
(20) Xiong, Y.; Luo, Y.; Li, H.; Wu, W.; Ruan, X.; Mu, X. Rapid Visual Detection of Dengue Virus by Combining Reverse Transcription Recombinase-Aided Amplification with Lateral-Flow Dipstick Assay. *International Journal of Infectious Diseases* **2020**, *95*, 406−412.
(21) Ross, G. M. S.; Filippini, D.; Nielen, M. W. F.; Salentijn, G. I. J. Unraveling the Hook Effect: A Comprehensive Study of High Antigen Concentration Effects in Sandwich Lateral Flow Immunoassays. *Anal. Chem.* **2020**, *92* (23), 15587−15595.
(22) Sathishkumar, N.; Toley, B. J. Development of an Experimental Method to Overcome the Hook Effect in Sandwich-Type Lateral Flow Immunoassays Guided by Computational Modelling. *Sens. Actuators, B* **2020**, *324*, 128756.
(23) Gasperino, D.; Baughman, T.; Hsieh, H. v; Bell, D.; Weigl, B. H. Improving Lateral Flow Assay Performance Using Computational Modeling. *Annu. Rev. Anal. Chem.* **2018**, 219.
(24) Berli, C. L. A.; Kler, P. A. A Quantitative Model for Lateral Flow Assays. *Microfluid. Nanofluid.* **2016**, *20* (7), 104.
(25) Rey, E. G.; O'Dell, D.; Mehta, S.; Erickson, D. Mitigating the Hook Effect in Lateral Flow Sandwich Immunoassays Using Real-Time Reaction Kinetics. *Anal. Chem.* **2017**, *89* (9), 5095−5100.
(26) Agarwal, P.; Toley, B. J. Unreacted PCR Primers Inhibit Signal in a Nucleic Acid Lateral Flow Assay: A Transport Reaction Model Elucidates. *nanoGe - EIMC*, July 20−21, 2021. https://www.nanoge.org/proceedings/EIMC/60d9b2b5574de60654130520 (accessed 2022-01-27).
(27) Rath, D.; Toley, B. J. Modeling-Guided Design of Paper Microfluidic Networks: A Case Study of Sequential Fluid Delivery. *ACS Sens.* **2020**, 91.

https://doi.org/10.1021/acsmeasuresciau.2c00005
ACS Meas. Sci. Au 2022, 2, 317−324